Mon. Not. R. Astron. Soc. **365,** 779–791 (2006) doi:10.1111/j.1365-2966.2005.09770.x

A new exact method for line radiative transfer

Moshe Elitzur[1]★ and Andrés Asensio Ramos[2]★

[1]*Department of Physics & Astronomy, University of Kentucky, Lexington, KY 40506, USA*
[2]*INAF–Osservatorio Astrofisico di Arcetri, Largo E. Fermi 5, 50125, Firenze, Italy*

Accepted 2005 October 11. Received 2005 October 10; in original form 2005 August 8

ABSTRACT

We present a new method, the coupled escape probability (CEP), for exact calculation of line emission from multi-level systems, solving only algebraic equations for the level populations. The CEP formulation of the classical two-level problem is a set of *linear equations*, and we uncover an exact analytic expression for the emission from two-level optically thick sources that holds as long as they are in the 'effectively thin' regime. In a comparative study of a number of standard problems, the CEP method outperformed the leading line transfer methods by substantial margins.

The algebraic equations employed by our new method are already incorporated in numerous codes based on the escape probability approximation. All that is required for an exact solution with these existing codes is to augment the expression for the escape probability with simple zone-coupling terms. As an application, we find that standard escape probability calculations generally produce the correct cooling emission by the C II 158-μm line but not by the ^{3}P lines of O I.

Key words: line: formation – radiative transfer – methods: numerical – ISM: lines and bands.

1 INTRODUCTION

Much of the information about astronomical sources comes from spectral lines, requiring reliable analysis of multi-level line emission. Most current methods for exact solutions involve accelerated Λ-iteration (ALI) techniques[1] in which the radiation intensity is obtained from the repeated action of an operator designated Λ on the source function (e.g. Rybicki 1991; Hubeny 1992). The ALI method utilizing short characteristics with parabolic interpolation of the source function (hereafter SCP: Olson, Auer & Buchler 1986) is a standard against which the efficiency of other line transfer techniques can be measured.

Because of the complexity and computational demands of exact methods, many simulation codes that attempt to implement as many realistic physical ingredients as possible are altogether bypassing solution of the radiative transfer equation, employing instead the escape probability technique. In this approach only the level populations are considered, calculated from rate equations that include photon escape factors which are meant to account approximately for the effects of radiative transfer [see Dumont et al. 2003 for a recent discussion and comparison with ALI calculations]. Since this approach is founded on a plausibility assumption right from the start, its results amount to an uncontrolled approximation without any means for internal error estimates. Nevertheless, this inherent shortcoming is often tolerated because of the simplicity and usefulness of the escape probability approach.

We present here a new exact method, the coupled escape probability (CEP), that retains all the advantages of the naive escape probability approach. In this new technique the source is divided into zones, and formal level population equations that are fully consistent with radiative transfer are derived rigorously from first principles. Different zones are coupled through terms resembling standard escape probability expressions, resulting in a set of level population equations with non-linear coefficients. Solution of this set of coupled algebraic equations produces level populations that are self-consistent with the line radiation they generate. Any desired level of accuracy can be achieved by increasing the number of zones.

We introduce our new method in Section 2. In Section 3 we study the two-level model in both a semi-infinite atmosphere and finite slabs, presenting results and comparison with SCP calculations. The new CEP method attains the exact solutions, outperforming the SCP method by substantial margins. We present the equations for multi-level systems in Section 4, and include as an example an application to the ^{3}P system of O I. Section 5 contains a discussion that, among other things, covers various technical details.

2 THE NEW TECHNIQUE

Consider the transfer of a line with frequency ν_0. The dimensionless line profile is $\Phi(x)$, normalized so that $\int \Phi(x)\,\mathrm{d}x = 1$, where $x = (\nu - \nu_0)/\Delta\nu_\mathrm{D}$ is the dimensionless frequency shift from line

★E-mail: moshe@pa.uky.edu (ME); aasensio@arcetri.astro.it (AAR)

[1] As noted by Trujillo Bueno & Fabiani Bendicho (1995), the ALI method is based on the Jacobi iteration (Jacobi 1845).

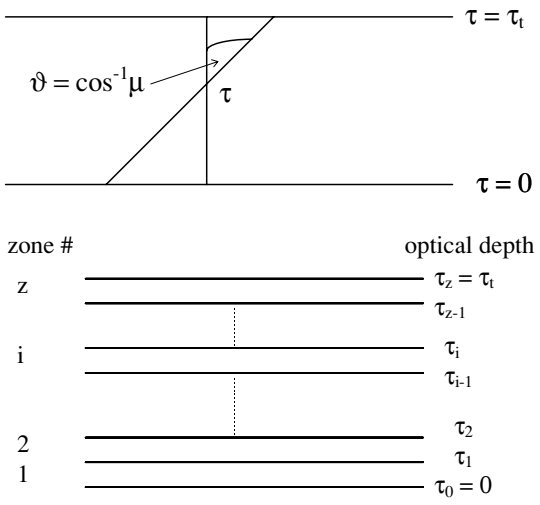

Figure 1. Top: sketch of the slab geometry for the radiative transfer problem. Bottom: the partition of the slab into zones (see Section 2.3).

centre and $\Delta\nu_{\rm D}$ is the Doppler width. We consider here only the case of $\Phi(x)$ that does not change its shape throughout the source and frequency-independent line source function S. These assumptions are adopted to simplify the presentation. They do not reflect inherent limitations of our new method.

2.1 Radiative transfer

For the geometry we adopt a plane-parallel slab the physical properties of which vary only perpendicular to the surface. Optical depth at frequency ν along a path orthogonal to the surface is $\tau_\nu = \tau\Phi(x)$, and τ can be used as a coordinate that uniquely specifies locations in the slab (see Fig. 1). The optical depth along a ray slanted at $\theta = \cos^{-1}\mu$ from normal is $\tau_\nu(\mu) = \tau\Phi(x)/\mu$, and the intensity along the ray obeys the radiative transfer equation

$$\mu\frac{{\rm d}I_\nu(\tau,\mu)}{{\rm d}\tau} = \Phi(x)[S(\tau) - I_\nu(\tau,\mu)]. \tag{1}$$

The equation for the flux $F_\nu = 2\pi\int I_\nu\mu\,{\rm d}\mu$ is obtained from integration over angles. The overall line flux $F = \int F_\nu\,{\rm d}\nu$ obeys at every position in the slab

$$\frac{{\rm d}F(\tau)}{{\rm d}\tau} = 4\pi\Delta\nu_{\rm D}[S(\tau) - \bar{J}(\tau)], \tag{2}$$

where

$$\bar{J}(\tau) = \int\frac{{\rm d}\Omega}{4\pi}\int I_\nu(\tau,\mu)\Phi(x)\,{\rm d}x \tag{3}$$

is the intensity averaged over both angles and line profile. Denoting by $\tau_{\rm t}$ the overall optical thickness and accounting for the emission from both faces of the slab, the line contribution to the cooling rate per unit area is

$$\Lambda = F(\tau_{\rm t}) - F(0) \equiv 4\pi\Delta\nu_{\rm D}J. \tag{4}$$

The line cooling factor J is introduced for convenience when $\Delta\nu_{\rm D}$ is constant in the slab. Integrating equation (2) over τ yields

$$J = \int_0^{\tau_{\rm t}} S(\tau)p(\tau)\,{\rm d}\tau. \tag{5}$$

Here we introduced

$$p(\tau) = 1 - \frac{\bar{J}(\tau)}{S(\tau)}, \tag{6}$$

a quantity that has been called the net radiative bracket (Athay & Skumanich 1971). From the formal solution of the radiative transfer equation,

$$p(\tau) = 1 - \frac{1}{2S(\tau)}\int_0^{\tau_{\rm t}} S(t)\,{\rm d}t\int_{-\infty}^{\infty}\Phi^2\,{\rm d}x\int_0^1 {\rm e}^{-|\tau-t|\Phi/\mu}\frac{{\rm d}\mu}{\mu} \tag{7}$$

when there is no external radiation entering the slab.

2.2 Level populations

Denote by $n_k(\tau)$, with $k = 1, 2$, the populations per sub-state of a given transition at position τ; that is, $n_k = N_k/g_k$ where g_k is the level degeneracy and N_k is the overall level population. Then the line source function is

$$S = \frac{A_{21}}{B_{21}}\frac{n_2}{n_1 - n_2}, \tag{8}$$

where A and B are the Einstein coefficients of the transition. The populations are obtained from steady-state rate equations of the form $\sum R_{ij} = 0$. The term corresponding to exchanges between the transition levels, separated by $E_{21} = h\nu_0$, is

$$R_{21} = -A_{21}n_2 - B_{21}\bar{J}(n_2 - n_1) - C_{21}\left(n_2 - n_1{\rm e}^{-E_{21}/kT}\right), \tag{9}$$

where C is the collision rate; exchanges with other levels have similar form and are listed in Section 4.

2.3 Solution

The common approach of exact solution methods is to handle radiative transfer and the level population distribution as two distinct problems, coupled through the results each of them gives. The problem is initialized with populations (and the corresponding source functions) obtained in some limiting case, e.g. thermal equilibrium. With these populations, radiative transfer (equation 1) is solved for the intensity to determine $\bar{J}$ (equation 3), which is then plugged into the rate terms (equation 9) to determine new populations, and so on. However, from equations (6) and (8), the rate term can be written as

$$R_{21} = -A_{21}n_2p - C_{21}\left(n_2 - n_1{\rm e}^{-E_{21}/kT}\right), \tag{10}$$

showing that the only radiative quantity actually needed for the calculation of level populations at every position is the net radiative bracket $p(\tau)$; given this factor we could compute the level populations that are consistent with the radiation they produce without solving for the intensity. And as is evident from equations (7) and (8), the factor $p(\tau)$ itself can be computed from the level populations, again without solving for the intensity. Therefore inserting $p(\tau)$ from equation (7) into the rate terms (equation 10) produces *level population equations that properly account for all the effects of radiative transfer without actually calculating the intensity itself*; the radiative transfer equation has been incorporated through its formal solution in equation (7).

A numerical solution of the resulting level population equations requires a spatial grid, partitioning the source into zones such that all properties can be considered uniform within each zone. The degree of actual deviations from uniformity, and the accuracy of the solution, can be controlled by decreasing each zone size through finer divisions with an increasing number of zones. Fig. 1 shows the slab partitioning into z zones. The ith zone, $i = 1 \ldots z$, occupies the

range $\tau_{i-1} < \tau \leqslant \tau_i$, with $\tau_0 = 0$ and $\tau_z = \tau_t$. The optical depth between any pair of zone boundaries is

$$\tau^{i,j} = |\tau_i - \tau_j| \tag{11}$$

so that the optical thickness of the ith zone is $\tau^{i,i-1}$. The temperature and collision rates are constant in the zone, and the corresponding rate term for its (constant) level populations is

$$R^i_{21} = -A_{21} n^i_2 p^i - C^i_{21} \left(n^i_2 - n^i_1 \mathrm{e}^{-E_{21}/kT_i} \right), \tag{12}$$

where the superscript i is used as a zone label. The factor $p(\tau)$ varies in the zone and has been replaced by a constant p^i that should adequately represent its value there, for example $p^i = \frac{1}{2}[p(\tau_i) + p(\tau_{i-1})]$ or $p^i = p[\frac{1}{2}(\tau_i + \tau_{i-1})]$. There are no set rules for this replacement other than it must obey $p^i \rightarrow p(\tau_i)$ when $\tau^{i,i-1} \rightarrow 0$. We choose for p^i the zone average

$$p^i = \frac{1}{\tau^{i,i-1}} \int_{\tau_{i-1}}^{\tau_i} p(\tau)\, \mathrm{d}\tau, \tag{13}$$

and this choice has proved to be very successful in our numerical calculations. From equation (7), calculation of p^i requires an integration over the entire slab, which can be broken into a sum of integrals over the zones. In each term of the sum, the zone source function can be pulled out of the τ-integration so that

$$p^i = 1 - \frac{1}{2\tau^{i,i-1} S^i} \sum_{j=1}^{z} S^j \times \int_{\tau_{i-1}}^{\tau_i} \mathrm{d}\tau \int_{\tau_{j-1}}^{\tau_j} \mathrm{d}t \int_{-\infty}^{\infty} \Phi^2\, \mathrm{d}x \int_0^1 \mathrm{e}^{-|\tau - t|\Phi/\mu} \frac{\mathrm{d}\mu}{\mu}. \tag{14}$$

The remaining integrals can be expressed in terms of common functions. Consider for example

$$\beta^i = 1 - \frac{1}{2\tau^{i,i-1}} \times \int_{\tau_{i-1}}^{\tau_i} \mathrm{d}\tau \int_{\tau_{i-1}}^{\tau_i} \mathrm{d}t \int_{-\infty}^{\infty} \Phi^2\, \mathrm{d}x \int_0^1 \mathrm{e}^{-|\tau - t|\Phi/\mu} \frac{\mathrm{d}\mu}{\mu}, \tag{15}$$

the contribution of zone i itself to p^i. It is straightforward to show that $\beta^i = \beta(\tau^{i,i-1})$, where

$$\beta(\tau) = \frac{1}{\tau} \int_0^{\tau} \mathrm{d}t \int_{-\infty}^{\infty} \Phi(x)\, \mathrm{d}x \int_0^1 \mathrm{d}\mu\, \mathrm{e}^{-t\Phi(x)/\mu}. \tag{16}$$

This function was first introduced by Capriotti (1965); it is the probability for photon escape from a slab of thickness τ, averaged over the photon direction, frequency and position in the slab. The contribution of zone $j \neq i$ to the remaining sum can be handled similarly, and the final expression for the coefficient p^i is

$$p^i = \beta^i + \frac{1}{\tau^{i,i-1}} \sum_{\substack{j=1 \\ j \neq i}}^{z} \frac{S^j}{S^i} M^{ij}, \tag{17}$$

where

$$M^{ij} = -\frac{1}{2}(\alpha^{i,j} - \alpha^{i-1,j} - \alpha^{i,j-1} + \alpha^{i-1,j-1}) \tag{18}$$

and where $\alpha^{i,j} = \tau^{i,j}\beta(\tau^{i,j})$. The quantity $\alpha^{i,j}$ obeys $\alpha^{i,j} = \alpha^{j,i}$ and $\alpha^{i,i} = 0$, therefore $M^{ij} = M^{ji}$ and $M^{ii} = \alpha^{i,i-1}$.[2] The first term in the expression for p^i is the average probability for photon escape from zone i, reproducing one of the common variants of the escape probability method in which the whole slab is treated as a single zone (e.g. Krolik & McKee 1978). The subsequent sum describes the effect on the level populations in zone i of radiation produced in all other zones. Each term in the sum has a simple interpretation in terms of the probability that photons generated elsewhere in the slab traverse every other zone and get absorbed in zone i, where their effect on the level populations is similar to that of radiation external to the slab (see Appendix A).

Inserting the coefficients p^i from equation (17) into the rate terms (equation 12) in every zone produces a set of non-linear algebraic equations for the unknown level populations n^i_k. The procedure was outlined here only for the diffuse radiation of a single transition; we describe the extension to multi-levels in Section 4 and the inclusion of external radiation in Appendix A. *Solution of these equations yields the full solution of the line transfer problem by considering only level populations*;[3] the computed populations are self-consistent with their internally generated radiation even though the radiative transfer equation is not handled at all. Once the populations are found, radiative quantities can be calculated in a straightforward manner from summations over the zones. The emerging intensity at direction μ is

$$I_\nu(\tau_t, \mu) = \sum_{i=1}^{z} \left(\mathrm{e}^{-\tau^{z,i}\Phi/\mu} - \mathrm{e}^{-\tau^{z,i-1}\Phi/\mu} \right) S^i. \tag{19}$$

The flux density emerging from each face of the slab obeys

$$\begin{aligned} F_\nu(\tau_t) &= 2\pi \sum_{i=1}^{z} \left[E_3(\tau^{z,i}\Phi) - E_3(\tau^{z,i-1}\Phi) \right] S^i, \\ -F_\nu(0) &= 2\pi \sum_{i=1}^{z} \left[E_3(\tau^{i-1,0}\Phi) - E_3(\tau^{i,0}\Phi) \right] S^i, \end{aligned} \tag{20}$$

where E_3 is the third exponential integral (e.g. Abramowitz & Stegun 1972). The line cooling coefficient is

$$J = \frac{1}{2} \sum_{i=1}^{z} (\alpha^{i,0} - \alpha^{i-1,0} - \alpha^{z,i} + \alpha^{z,i-1}) S^i. \tag{21}$$

The solution method just described is exact – the discretized equations are mathematically identical to the original ones when $\tau^{i,i-1} \rightarrow 0$ for every i. As is usually the case, the only approximation in actual numerical calculations is the finite size of the discretization, i.e. the finite number of zones. A desired accuracy is achieved when, upon further division, the relative change in all level populations is smaller than the prescribed tolerance.

2.4 Numerical implementation

The level populations of all zones are described by a set of non-linear algebraic equations. The equations are readily solved by the Newton method, which utilizes the Jacobian of the set. Since the dependence on the unknown variables is explicit in all the rate terms, the Jacobian can be computed from analytic expressions. The functions β (see equation 16), $\alpha = \tau\beta$ and their derivatives are conveniently

[2] Since $\beta^i = M^{ii}/\tau^{i,i-1}$, the first term could be incorporated into the sum in equation (17) as the $j = i$ term.

[3] Apruzese et al. (1980) proposed somewhat similar equations. They based their arguments on probabilistic reasoning and did not offer a formal derivation. We thank P. Lockett for bringing this to our attention.

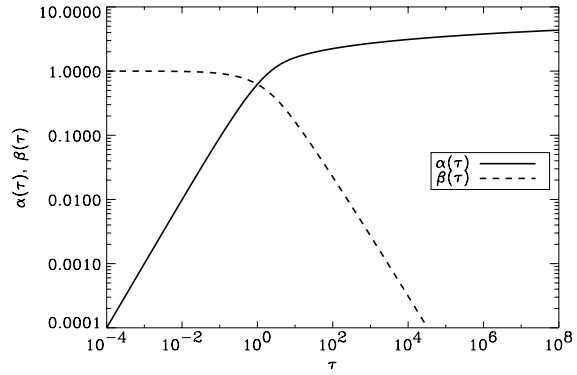

Figure 2. Plots of the functions β (see equation 16) and $\alpha = \tau\beta$ (equation 22).

calculated from the representations

$$\alpha(\tau) = \int_{-\infty}^{\infty} \mathrm{d}x \left\{ \frac{1}{2} - E_3[\tau\Phi(x)] \right\},$$
$$\alpha'(\tau) = \int_{-\infty}^{\infty} \Phi(x) E_2[\tau\Phi(x)]\,\mathrm{d}x, \qquad (22)$$

where E_2 is the second exponential integral. Fig. 2 plots β and α. While β is a monotonically decreasing function, α is monotonically increasing and its asymptotic behaviour when $\tau \to \infty$ is $\alpha \sim \sqrt{\ln \tau}$. This divergent behaviour does not pose any problems because α cancels to first order in the thickness of the zones in the linear combinations defining M^{ij} (equation 18). Only the second-order terms, involving the second derivative α'', survive.

Since our aim is to explore the intrinsic accuracy of our new method, the integrals in equation (22) were computed repeatedly with an 80-point Gaussian quadrature to ensure that these integrations do not compromise the precision of the outcome. The E_n functions were evaluated with a rapidly convergent series from Press et al. (1986). The integration range was truncated at $x = \pm 7$, which we have verified is sufficient in all cases thanks to the rapid decrease with x of the integrands.

In order to test the new method, the radiative transfer problem was also solved using the ALI method for comparison. The technique is based on a modified Λ iteration in which the statistical equilibrium equations are linearized via the Rybicki & Hummer (1992) pre-conditioning scheme. The method also takes advantage of an operator splitting scheme by introducing an approximate operator Λ^*, the diagonal of the exact operator Λ in the formal solution $\bar{J} = \Lambda[S]$ of the radiative transfer equation. It has been shown that the introduction of this operator leads to an optimal balance between the convergence rate and computing time per iteration (Olson et al. 1986; Carlsson 1991). The ALI calculations presented in this paper utilize a formal solver based on the short-characteristics scheme with parabolic precision (Olson et al. 1986), currently considered the method of choice for complicated line transfer problems (e.g. Kunasz & Auer 1988; Auer, Fabiani Bendich & Trujillo Bueno 1994; van Noort, Hubeny & Lanz 2002; Fabiani Bendicho 2003). With this SCP method, equation (1) was solved for many frequencies and ray inclinations, and the mean intensity computed from angular and frequency integrations (equation 3) by numerical quadratures.[4] To ensure the high precision required in this comparative study, the angular integration was done with a Gaussian quadrature with 24 points in the variable μ. The frequency integrals were done with trapezoidal integration extending to $x = \pm 4$ with 33 frequency points, which we have verified yields the desired precision.

We proceed now to present solutions and comparisons of the newly developed CEP method with the SCP method for a number of standard problems. In all the examples we employ uniform physical conditions and the Doppler shape for the line profile, $\Phi = \pi^{-1/2}\mathrm{e}^{-x^2}$; note that the line centre optical depth is then $\tau_0 = \tau/\sqrt{\pi}$.

3 TWO-LEVEL ATOM

In the two-level problem, the steady-state rate equation $R_{21} = 0$ (equation 9) yields the familiar expression for the source function

$$S = (1-\epsilon)\bar{J} + \epsilon B(T), \qquad (23)$$

where B is the Planck function and where

$$\frac{\epsilon}{1-\epsilon} = \frac{C_{21}}{A_{21}}(1 - \mathrm{e}^{-E_{21}/kT}) \equiv \frac{N}{N'_{\mathrm{cr}}}. \qquad (24)$$

Here N is the density of the collision partners and N'_{cr} the standard critical density with a slight modification that incorporates the Boltzmann factor correction. Replacing $\bar{J}$ with p (equation 6), the equation for the source function becomes

$$(1+\eta p)S = B, \qquad \text{where} \qquad \eta = \frac{N'_{\mathrm{cr}}}{N}; \qquad (25)$$

this result also follows directly from equation (10) with $R_{21} = 0$. When the two-level problem is formulated with optical depth as the independent variable, it is fully characterized by the two input quantities $B(T)$ and ϵ (or, equivalently, η) specified as functions of τ. There is no need to specify intrinsic properties of the transition such as, for example, E_{21} or A_{21}. Instead of solving for the population of each of the two levels, this single equation for the unknown S provides the complete solution of the problem.

Dividing the slab into zones, the rate equation $R^i_{21} = 0$ (equation 12) produces a similar expression for the ith zone,

$$S^i + \eta^i p^i S^i = B(T^i), \qquad (26)$$

with η^i and T^i corresponding to the physical conditions in the zone. Inserting the expression for p^i from equation (17), the CEP set of equations for the unknown S^i is

$$(1+\eta^i\beta^i)S^i + \frac{\eta^i}{\tau^{i,i-1}} \sum_{\substack{j=1 \\ j\neq i}}^{z} M^{ij} S^j = B(T^i). \qquad (27)$$

Since the factors β^i and M^{ij} depend only on optical depth, they are independent of the unknown variables (the zone source functions S^i) in this case. Therefore *the CEP technique transforms the two-level problem to a set of linear equations*. This is a reflection of the linear relation between I_ν and S in equation (1) which is maintained when the complete problem is handled in terms of optical depth as the independent variable. The CEP formulation produces directly the explicit linear equations in this case.

We proceed now with solutions for semi-infinite atmospheres and finite-thickness slabs with constant physical conditions. When the temperature is constant, $B(T)$ merely sets the intensity scale and only the dependence on ϵ need be studied.

[4] It is interesting to note that the calculation of the mean intensity has also been done using Monte Carlo techniques (see e.g. van Zadelhoff et al. 2002 and references therein).

3.1 Semi-infinite atmosphere

We start with the classical problem of a stellar atmosphere, where τ measures distance from the surface and $\tau_{\rm t} \to \infty$. The source function is subject in this case to the exact limits

$$S \to B \times \begin{cases} \sqrt{\epsilon} & \text{when } \tau \to 0 \\ 1 & \text{when } \tau \gg 1/\epsilon \end{cases} \tag{28}$$

(e.g. Avrett & Hummer 1965). In order to capture both limit behaviours we model the atmosphere as a slab divided logarithmically into z zones that cover 10 orders of magnitude in optical depth from $\tau = 10^{-3}$ to $\tau_{\rm t} = 10^{7}$, with the latter serving as a proxy for the atmospheric interior. The two faces of the slab are a priori identical. When the radiative transfer equation is part of the calculation, this two-sided symmetry is broken by the boundary condition $I_\nu(\tau = \tau_{\rm t}, \mu) = 0$, which introduces a radiation sink at the $\tau_{\rm t}$-boundary. This is the case in ALI methods, including SCP. The CEP method, on the other hand, does not involve the radiation at all and thus cannot invoke boundary conditions to differentiate between the two slab faces. Instead, this is accomplished by the logarithmic division that starts at one end, and the great disparity that this introduces between photon escape from the two sides. The semi-infinite atmosphere could also be mimicked by doubling the slab with its mirror image and considering the source function only between one surface and the mid-plane. We have verified that the results of calculations with the two approaches are practically identical. In order to compare the CEP method with SCP under identical conditions, we present the results for logarithmic divisions increasing toward the slab surface at $\tau_{\rm t}$.

Fig. 3 shows the results for some representative models, ranging from $\epsilon = 10^{-5}$ ($N = 10^{-5}\ N'_{\rm cr}$) to $\epsilon = 0.5$ ($N = N'_{\rm cr}$). For example, the Ca II H line can be modelled in a 5000-K atmosphere with $\epsilon = 3.65 \times 10^{-5}$ (e.g. Avrett & Loeser 1987, and references therein). The top panel of each plot shows the solution obtained with the SCP method with 3000 zones, displaying the proper limit behaviour at both ends of the optical depth axis. The CEP method attains these solutions with a sufficient number of zones, validating our new technique. However, the convergence with z is quite different for the two methods.

At the surface, the SCP method is close to the exact solution already at $z = 20$ (only two zones per logarithmic decade) in all cases; the deviation is less than 40 per cent at $\epsilon = 10^{-5}$ and decreases further as ϵ increases. Increasing z brings rapid convergence. In contrast, deep inside, the rate of convergence is much more moderate. Furthermore, when ϵ increases, both the magnitude of deviations and the rate of convergence around $\tau \sim 10$ remain almost the same for all $\epsilon \leqslant 0.1$. The behaviour at both ends reflects the short-characteristics nature of the method, in which only nearby regions are coupled, and the fact that the radiative transfer equation is always solved. Radiative transfer effects are minimal at small τ, which is why the method attains easily the exact solution near the surface. However, the effects are significant at the optical depths where the transition to thermalization occurs, the radiative transfer equation must be repeatedly solved and the convergence in these regions is hardly improved by the increase in collision rates as long as N remains subcritical.

In an almost mirror behaviour, at the surface the CEP method deviates from the exact solution by more than factor of 2 at $z < 100$ when ϵ is small, and its convergence rate to the exact solution is slow there. However, deep inside the atmosphere, the deviations are actually smaller than at the surface. Moreover, when ϵ increases, the deviations decrease everywhere. At $\epsilon = 0.1$, the CEP method

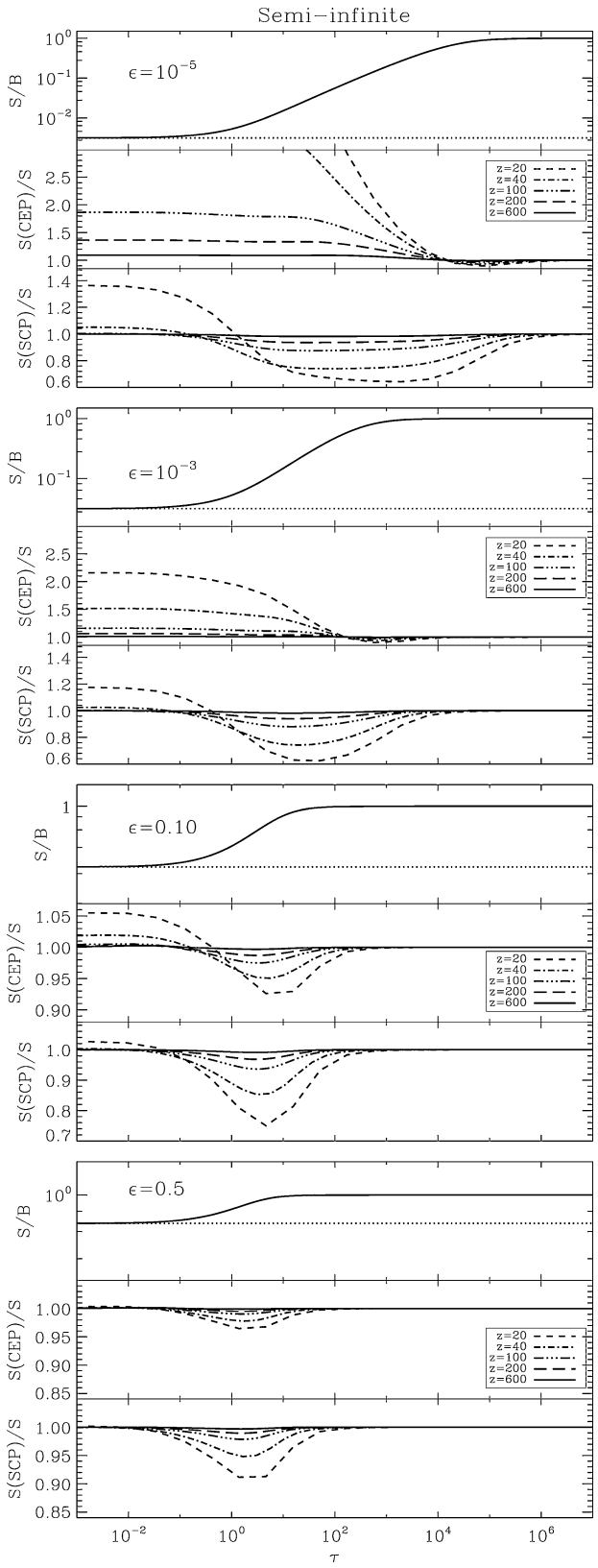

Figure 3. The two-level model with various values of ϵ (equation 24) in a semi-infinite atmosphere. The top panel of each plot shows the variation of the source function with depth into the atmosphere. The two other panels show the convergence to the exact solution as the number of zones z is increased for the CEP and SCP methods. Note the change in scale of the vertical axis between different panels.

Table 1. Runtime (in seconds, on the same computer) required by the SCP and CEP methods to solve an atmosphere with $\epsilon = 10^{-3}$ for the number of zones listed in the first column; in the SCP method this corresponds to the number of grid points. Omitted entries were too short for meaningful timing. The listed error is the percentage deviation from the result of an SCP calculation with 3000 zones.

Zones	Time		Percentage error	
	SCP	CEP	SCP	CEP
20	0.39	–	36.3	103.6
40	1.10	–	23.9	45.7
100	4.39	0.006	10.9	14.0
200	11.6	0.089	5.5	5.4
600	44.9	1.70	1.6	1.2

is within 7 per cent of the exact solution everywhere already at $z = 20$; in contrast, this accuracy is attained by the SCP method only at $z = 100$. These properties are readily understood from the CEP formalism. Since the level population equations couple the entire atmosphere, the surface layers are affected by the behaviour deep inside. Also, because the radiative transfer equation is avoided altogether, the method takes full advantage of the thermalization that approaches the surface when ϵ increases.

Performance statistics for the two methods are summarized in Table 1 for the case $\epsilon = 10^{-3}$; the statistics for other cases show similar trends. The CEP technique attains the solution much more quickly than the SCP method in all cases.

3.2 Finite-thickness slabs

One of the main coolants of photodissociation regions (PDRs) is the 158-μm line of C II, the emission of which is often modelled with a simple escape probability approximation of the two-level system (e.g. Tielens & Hollenbach 1985). When this approach employs the Capriotti expression for the escape probability (equation 16), it is identical to a CEP calculation with only one zone. For comparison with exact solutions, we include such single-zone CEP calculations in the results presented here. The numerical calculations employ z zones of equal thickness.

Fig. 4 shows the variation of the source function inside slabs of various optical thickness for $\epsilon = 10^{-5}$. The displayed behaviour is representative of all $N \ll N'_{\rm cr}$ cases. The results of single-zone CEP calculations provide reasonable approximations at small $\tau_{\rm t}$, but become poorer as the variation range of the source function gets wider with increasing $\tau_{\rm t}$. However, with only 20 zones the CEP results are within 1 per cent of the exact solution everywhere when $\tau_{\rm t} \leqslant 10$, 4 per cent when $\tau_{\rm t} \leqslant 50$ and 10 per cent when $\tau_{\rm t} \leqslant 100$. An accuracy better than 10 per cent is always achieved when the optical thickness of each zone is $\lesssim 5$. In contrast, the SCP method does not reach this level of accuracy near the surface of a $\tau_{\rm t} = 500$ slab even with 200 zones; as a grid- rather than zone-based method, it attempts to resolve the surface structure even when that is not required. Furthermore, SCP calculations require a large number of divisions even at moderate optical thickness; when $\tau_{\rm t} = 10$, a 10 per cent accuracy requires 100 zones. The reason, as noted above, is that the equation of radiative transfer must be solved repeatedly; the approach to thermal equilibrium of level populations deep inside the slab does not alleviate this need, and large optical depths dictate a large number of zones.

Since the CEP technique employs only level populations, it takes full advantage of level thermalization. The difference from standard

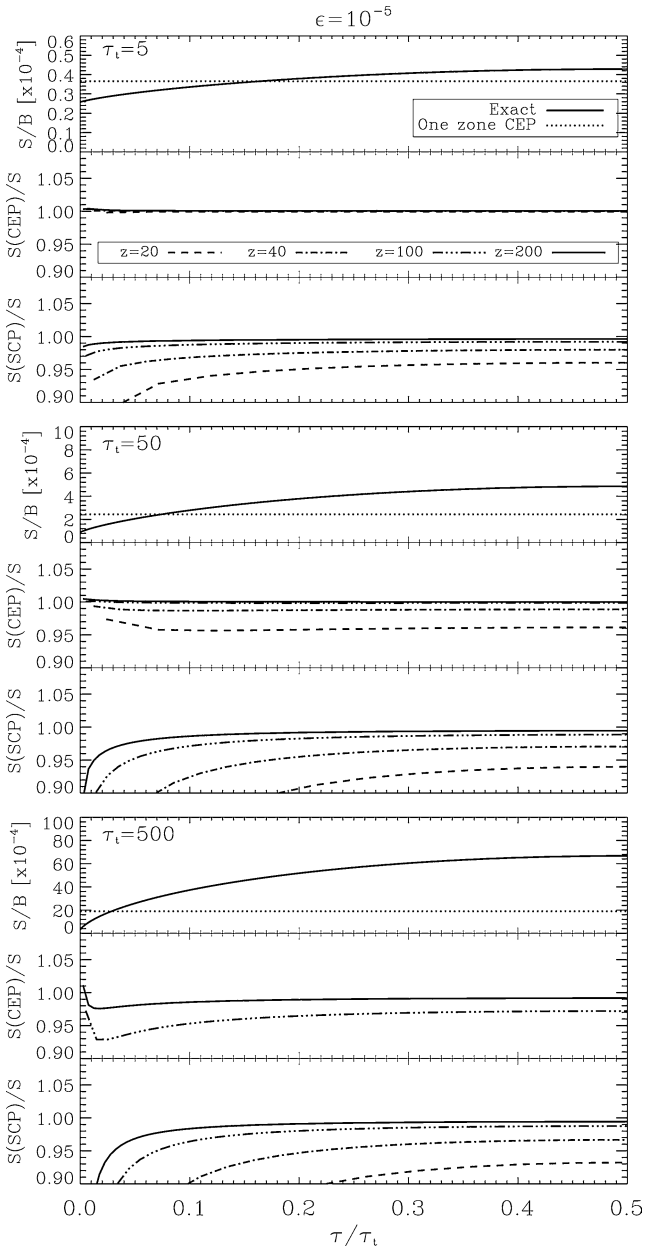

Figure 4. The two-level model with $\epsilon = 10^{-5}$ in slabs with overall optical thickness $\tau_{\rm t}$. The top panel of each plot shows the variation of the source function from the surface to the slab mid-plane in the exact solution and in a single-zone CEP calculation. The two other panels show the convergence to the exact solution with the number of zones z for the CEP and SCP methods.

methods in the case of $\epsilon = 0.5 (N = N'_{\rm cr})$, shown in Fig. 5, is striking. Already with one zone, CEP calculations produce acceptable results inside every slab, even with $\tau_{\rm t}$ as large as 500; 20 zones suffice for 3 per cent accuracy everywhere. In contrast, to achieve 10 per cent accuracy, SCP requires 100 zones at a moderate $\tau_{\rm t} = 50$, and even 200 zones are insufficient when $\tau_{\rm t} = 500$. The zone thicknesses in this case is $\tau = 2.5$, enough to challenge numerical solutions of the radiative transfer equation that SCP must perform.

Table 2 summarizes the performance statistics in one representative case. The CEP method outperforms SCP by an even larger margin than in the case of an atmosphere.

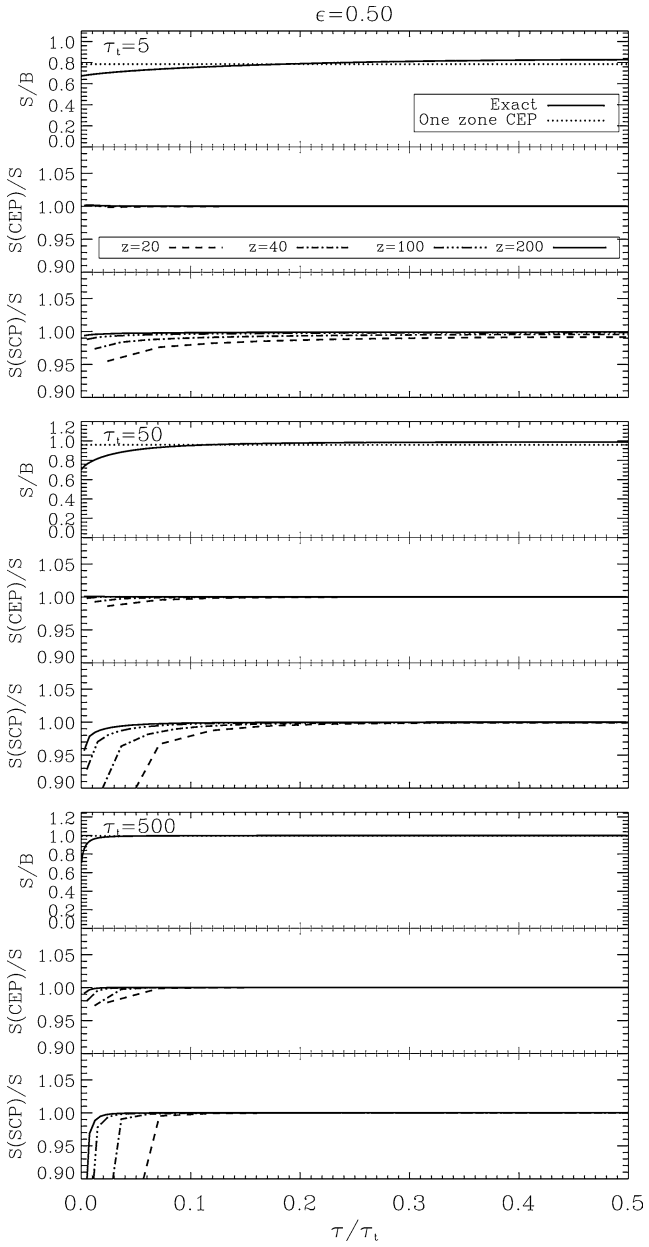

Figure 5. As Fig. 4, only with $\epsilon = 0.5$.

3.2.1 *Slab emissivity*

The advantages offered by the CEP method are even more pronounced for slab emission calculations. Fig. 6 shows a striking result: when $\epsilon = 10^{-5}$ (i.e. $\eta = 10^5$), the CEP method produces with a single zone the correct line cooling coefficient for all slabs with $\tau_t \leqslant 500$! This result is easy to understand. From the behaviour of the function β at small and large τ (Capriotti 1965), it follows that $p(\tau) \sim 1$ when $\tau < 1$ and that $p(\tau) \sim 1/\tau$ when $\tau \gg 1$, so that $p(\tau) \gtrsim 1/\tau_t$. Therefore slabs with $\eta > \tau_t$ have $\eta p > 1$ everywhere. From equations (25) and (5) it follows that in this case

$$\tau_t \ll \eta: \quad S(\tau) = \frac{B}{\eta p}, \qquad J(\tau_t) = \int_0^{\tau_t} \frac{1}{\eta} B d\tau. \tag{29}$$

The expression for J involves only input properties. That is, *the line cooling coefficient can be calculated in this regime without even solving the problem*. This result does not seem to have been recognized in the published literature. When the physical conditions are constant, $J = B\tau_t/\eta$; the source is optically thick yet its emission increases linearly with optical depth. The slab remains 'effectively thin' at large optical depths as long as $\tau_t \ll \eta$ (i.e. $\epsilon\tau_t \ll 1$). And because the CEP method employs discretized forms of these expressions, it reproduces the correct line emission irrespectively of the division into zones.

Table 2. Performance comparison of the SCP and CEP methods, similar to Table 1, for a slab with $\epsilon = 10^{-3}$ and $\tau_t = 500$. The listed errors include the percentage deviations of both the source function and the line cooling coefficient from the exact results.

	Time		Percentage error – S		Percentage error – J	
Zones	SCP	CEP	SCP	CEP	SCP	CEP
1	0.03	–	99.5	55.5	98.6	25.0
10	0.60	–	93.3	31.0	28.2	13.2
20	1.02	–	88.2	23.0	17.5	7.94
40	3.29	–	79.8	15.5	10.1	4.01
100	12.6	0.033	62.5	6.47	3.94	1.21
200	28.1	0.085	46.4	2.22	1.60	0.40

Since $J(\tau_t)$ can be calculated without solving any equations, the single-zone calculation produces the correct emission even though it does not reproduce the correct population distribution – as is evident from both equation (29) and Fig. 4, the source function varies in the slab while the one-zone result is constant. Still, this constant value is just the right average to reproduce the slab luminosity correctly. Another perspective on this result is provided by the spectral shape of the emergent radiation, shown in Fig. 7. The exact solution properly displays a self-absorption dip around line centre (see e.g. Avrett & Hummer 1965). The single-zone calculation is incapable of producing this feature, but its flat-top shape does enclose the same area, reproducing the correct line luminosity. The simple one-zone calculation properly reproduces the overall number of photons emitted in the line, although not the frequencies where they emerge.

When the problem is formulated in terms of τ, equation (29) gives the line emission directly from the input properties. When the problem is formulated instead in terms of densities and distances, equation (29) implies that[5]

$$\Lambda = E_{21} \int g_1 C_{12} (n_1 - n_2) \, \mathrm{d}\ell. \tag{30}$$

Although the condition $\eta p > 1$ ensures that $n_2 \ll n_1$ when $E_{21} > kT$, n_2 need not be negligible when $E_{21} < kT$. Therefore the solution must be executed in this case to determine the population distribution and the actual value of τ_t. Since the single-zone calculation does not produce the correct population distribution, its result for the overall optical depth can be wrong. To ensure the correct assignment of τ_t to the prescribed input, the problem must be solved properly, including the division into zones.

When ϵ increases, the slab ceases to be 'effectively thin' and the line luminosity begins to deviate from the one-zone CEP result, as is evident from Fig. 6. Eventually, linethermalization sets in with further increase in ϵ, and the single-zone result again becomes

[5] This result was noticed in the limit in which $n_2 \ll n_1$ by D. Neufeld in benchmark testing of radiative transfer codes, posted at http://www.mpifr-bonn.mpg.de/staff/fvandertak/H2O/radxfrtest.pdf. Note that the line cooling always obeys $\Lambda = E_{21} \int (C_{12}N_1 - C_{21}N_2) \, \mathrm{d}\ell = E_{21} \int g_1 C_{12} (n_1 - n_2 e^{E_{21}/kT}) \, \mathrm{d}\ell$, as is evident from equations (5), (8) and (10).

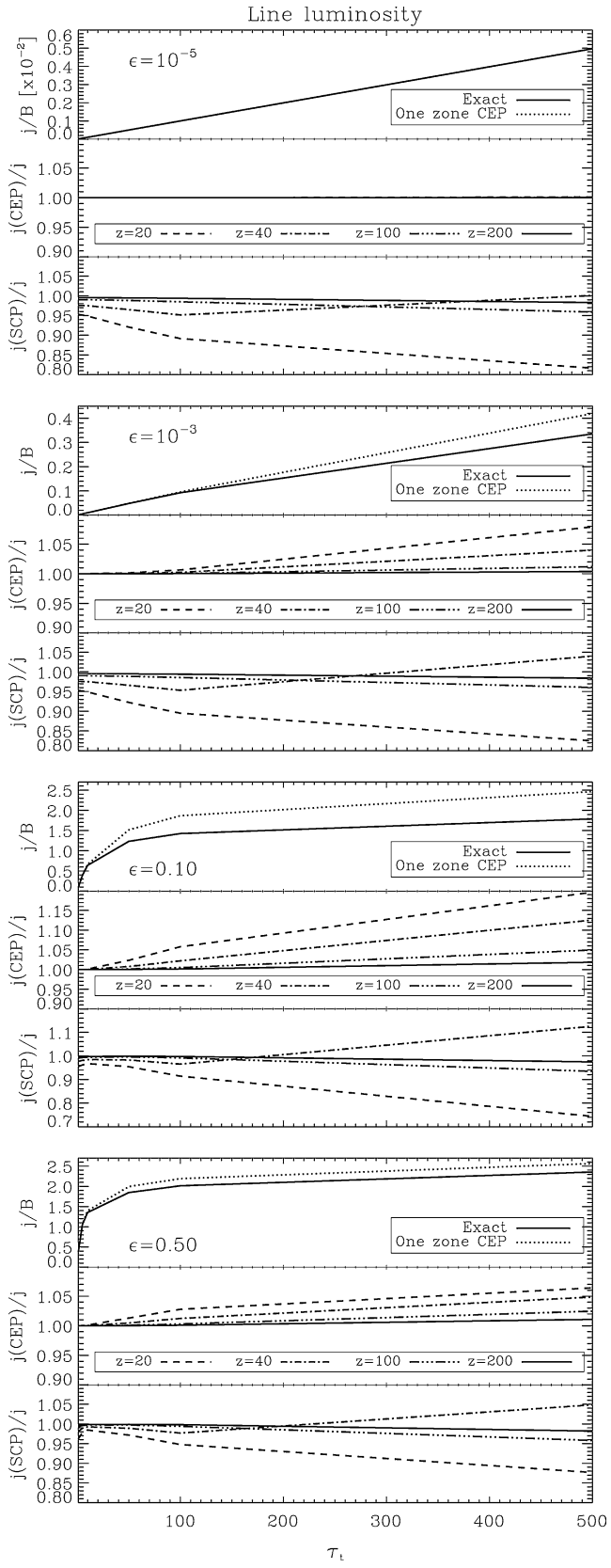

Figure 6. The line cooling coefficient of a slab as a function of its overall optical depth in two-level models with various ϵ. The top panel of each plot shows the exact solution and the result of a single-zone CEP calculation. The two other panels show the convergence to the exact solution with the number of zones z for the CEP and SCP methods.

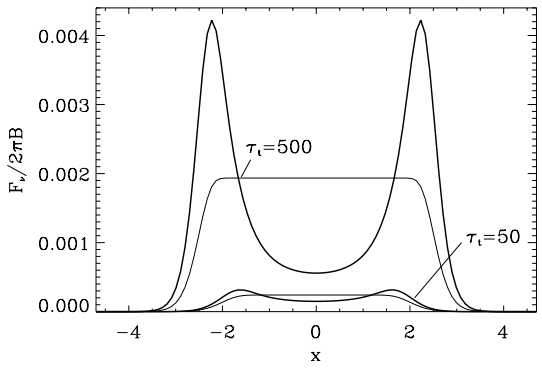

Figure 7. Spectral shape of the flux emerging from slabs with $\epsilon = 10^{-5}$ and optical depths as marked. The thick lines are the result of the exact solution, the thin lines of a single-zone CEP calculation.

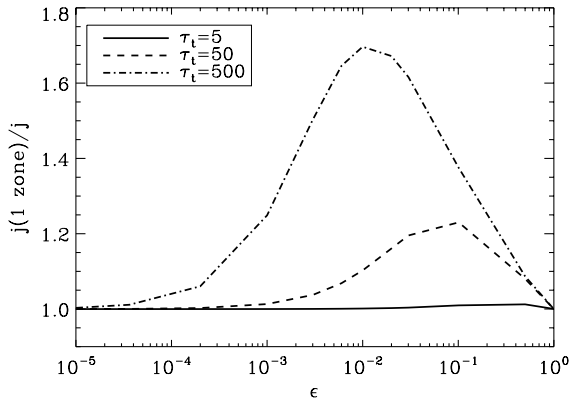

Figure 8. Deviation of the one-zone CEP result from the exact value of the line cooling coefficient as a function of ϵ in two-level models with various slab thicknesses.

adequate. This behaviour is further illustrated in Fig. 8. At a fixed τ_t, the deviation from the single-zone CEP calculation reaches a maximum when $\epsilon \sim 5/\tau_t$. When $\tau_t = 50$ the maximal deviation is ∼20 per cent at $\epsilon \sim 0.1$; when $\tau_t = 500$ it is ∼70 per cent at $\epsilon \sim 0.01$. Varying ϵ away from that peak in either direction, the one-zone CEP calculation gives a progressively better approximation.

With $N'_{cr} = 4 \times 10^3$ cm^{-3} at $T = 75$ K, the 158-μm line of C II is in the regime $N \gtrsim N'_{cr}$ ($\epsilon \gtrsim 0.5$) in most cases of interest. Therefore single-zone CEP calculations for this line are expected to produce cooling rates accurate to better than ∼10 per cent under most circumstances.

4 MULTI-LEVEL SYSTEMS

Consider L energy levels. A trivial change from the two-level case is the addition of some bookkeeping indices. We designate level numbers with subscripts and zone numbers with superscripts. In zone i, the population per sub-state of level k is n_k^i and the overall population is

$$n^i = \sum_{k=1}^{L} g_k n_k^i, \tag{31}$$

where g_k is the level degeneracy. Unlike the two-level system, locations in the slab cannot be specified by optical depth anymore because each transition has a different optical depth, which can be determined only after the unknown n_k^i are calculated. Instead, the

partition into zones is done in terms of the geometrical distance from one surface. Denote by ℓ^i the width of the ith zone, then its optical thickness in the transition between lower level l and upper level u is

$$\tau_{ul}^{i,i-1} = \frac{1}{4\pi\Delta\nu_{\rm D}} g_u B_{ul} E_{ul} \left(n_l^i - n_u^i\right) \ell^i, \tag{32}$$

where E_{ul} is the energy separation between levels u and l. The equivalent of equation (11) is then

$$\tau_{ul}^{i,j} = \sum_{k=j+1}^{i} \tau_{ul}^{k,k-1} \tag{33}$$

when $i > j$. In complete analogy with equations (12), (17) and (18), the level population equations are

$$\frac{{\rm d}n_k^i}{{\rm d}t} = -\sum_{l=1}^{k-1} A_{kl}\, p_{kl}^i n_k^i + C_{kl}^i \left(n_k^i - n_l^i {\rm e}^{-E_{kl}/kT^i}\right) + \sum_{u=k+1}^{L} \frac{g_u}{g_k} \left[A_{uk}\, p_{uk}^i n_u^i + C_{uk}^i \left(n_u^i - n_k^i {\rm e}^{-E_{uk}/kT^i}\right)\right]. \tag{34}$$

Here

$$p_{ul}^i = \beta_{ul}^i + \frac{1}{\tau_{ul}^{i,i-1}} \sum_{\substack{j=1 \\ j\neq i}}^{z} \frac{n_u^j}{n_u^i} \frac{n_l^i - n_u^i}{n_l^j - n_u^j} M_{ul}^{ij}, \tag{35}$$

where

$$M_{ul}^{ij} = -\frac{1}{2}\left(\alpha_{ul}^{i,j} - \alpha_{ul}^{i-1,j} - \alpha_{ul}^{i,j-1} + \alpha_{ul}^{i-1,j-1}\right) \tag{36}$$

and where $\beta_{ul}^i = \beta(\tau_{ul}^{i,i-1})$ and $\alpha_{ul}^{i,j} = \tau_{ul}^{i,j}\ \beta(\tau_{ul}^{i,j})$. This provides a set of $L-1$ independent equations for the L unknown populations in each zone, n_k^i. Equation (31) for the overall density in the zone closes the system. The overall system of non-linear algebraic equations for the level populations in all zones is readily solved with the Newton method.

It is convenient to switch to the scaled quantities n_k^i/n^i as the unknown variables and introduce the overall column density

$$\mathcal{N} = \sum_{i=1}^{z} n^i \ell^i. \tag{37}$$

Neither densities nor physical dimensions need then be specified since only $\mathcal{N}$ enters as an independent variable; the zone partition is done in terms of $\mathcal{N}$ rather than ℓ. The problem is fully specified by three input parameters: density N of collision partners and temperature T, which together determine the collision terms, and $\mathcal{N}$ (in fact, $\mathcal{N}/\Delta\nu_{\rm D}$), which sets the scale for all optical depths.

4.1 Example – the O I cooling lines

Together with C II 158 μm, the ^{3}P lines of O I at 63 and 145 μm dominate the gas cooling of warm PDRs. Ratios and peak intensities of these lines are used to measure the gas density and temperature (Tielens & Hollenbach 1985). In Section 3.2.1 we found that simple escape probability calculations do reproduce the proper C II 158-μm emission. We now examine the behaviour of O I lines through an exact CEP calculation of the three levels of the ^{3}P system. We solve for slabs with constant physical conditions, specified by temperature, hydrogen density and oxygen column density $\mathcal{N}(O)$.

Fig. 9 shows the effect of varying the number of zones on the cooling line emission at $T = 100$ K; the results are similar for

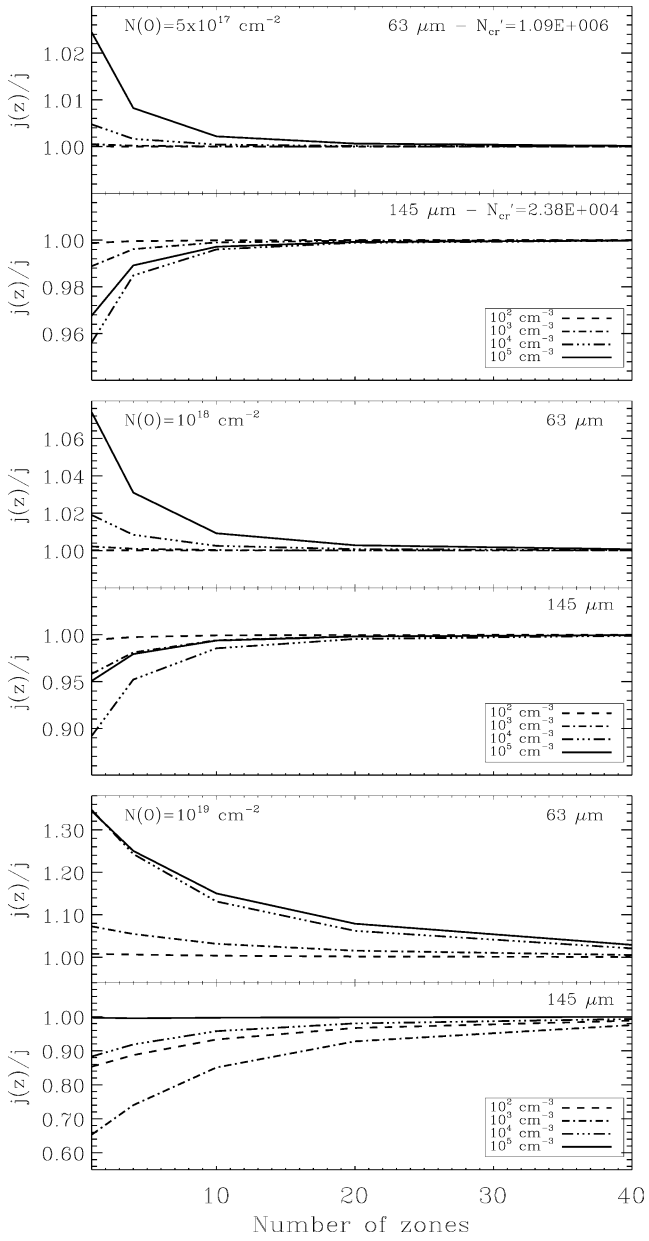

Figure 9. Variation of the emission in the ^{3}P cooling lines of O I with the number of zones in CEP calculations. Shown are the ratios to the exact solutions for slabs with $T = 100$ K, various H densities, as marked, and three representative oxygen column densities. At $\mathcal{N}({\rm O}) \leqslant 10^{17}$ cm^{-2}, the single-zone calculation produces the exact result for both lines. The critical density for each line is listed in the top figure.

$T = 300$ and 500 K.[6] Single-zone CEP calculations produce the exact result at $\mathcal{N}({\rm O}) \leqslant 10^{17}$ cm^{-2}, but deviate from it at larger column densities by amounts that increase with $\mathcal{N}$(O). The deviation is different for each line, reflecting their different critical densities, which are listed in the figure, and optical depths; for reference, at $\mathcal{N}({\rm O}) = 10^{19}$ cm^{-2}, $\tau(63\ \mu{\rm m}) \sim 100$ while $\tau(145\ \mu{\rm m})$ varies from

[6] It is interesting to note that the 145-μm transition undergoes population inversion in the optically thin regime at low densities for temperatures above 300 K. The reason is that the radiative lifetime of its upper level is more than five times longer than for its lower level.

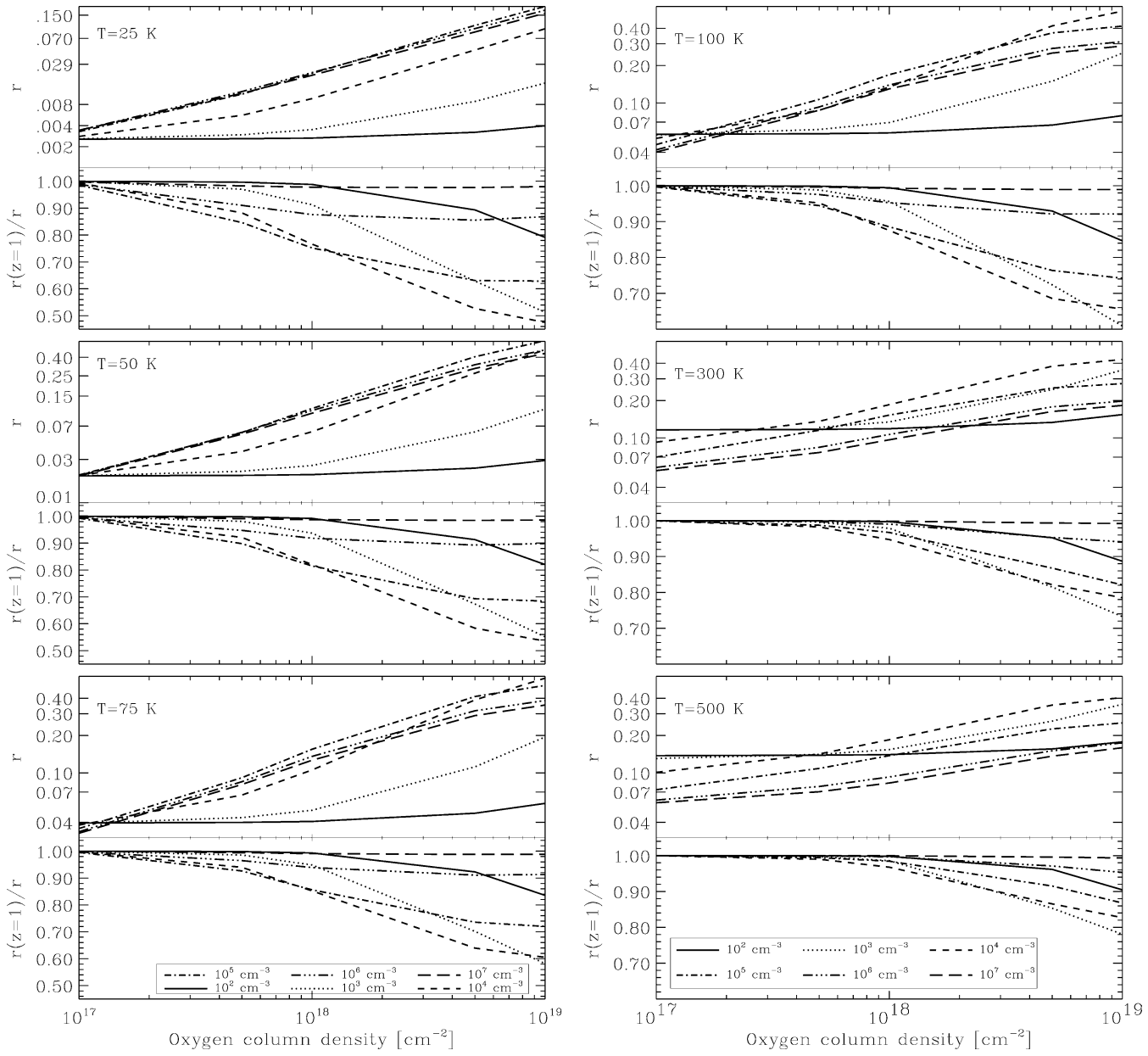

Figure 10. The ratio $r = \jmath(145\ \mu\text{m})/\jmath(63\ \mu\text{m})$ of the O I cooling lines as a function of oxygen column density for various temperatures and H densities, as marked. The top panel in each case shows the exact ratio r, the bottom panel the ratio of the results of single-zone calculations to the exact ones.

$\sim$0.6 to $\sim$2, depending on the density. Because of the different trends displayed by the emission in the two cooling lines, the one-zone calculation generally misses the exact result for their ratio $r = \jmath(145\ \mu\text{m})/\jmath(63\ \mu\text{m})$. Fig. 10 shows the variation of r with column density and the deviations of the results of a one-zone calculation from the exact values. The single-zone results differ from the exact values by amounts that vary with temperature, density and oxygen column density. The deviations are generally largest at hydrogen densities around 10^3–10^4 cm^{-3}. As is evident from this figure, the variation range of r is comparable to the error that can be introduced by its calculation with a single zone. A reliance on such calculations can lead to erroneous conclusions regarding the physical conditions in a source. Indeed, from the observed ratio of the two [O I] lines and escape probability calculations, Caux et al. (1999) deduced a mean gas temperature of 26 ± 0.5 K, an H_2 density $\geqslant 3 \times 10^4$ cm^{-3} and an [O I] column density $\geqslant 5 \times 10^{19}$ cm^{-2}. However, as is evident from Fig. 10, the large values which they observed ($r \sim 0.4$) can be reached at lower columns for a wide range of somewhat higher temperatures.

One-zone CEP calculations of the O I cooling lines are not as reliable as they are for the C II 158-μm emission. However, it does not take too many zones for the CEP method to achieve adequate accuracy. As is evident from Fig. 9, 20 zones suffice for accomplishing better than 10 per cent accuracy, and the exact solution is reached to within 1 per cent with 40 zones in all cases.

5 DISCUSSION

The test cases presented here show that our new method not only provides an exact solution of the line transfer problem, but it also

outperforms the leading ALI solver by a margin even larger than that among different implementations of the ALI technique. Two fundamental properties give the CEP method intrinsic advantages. The first is the calculation of $\bar{J}$, the only radiative quantity required for solving the level populations. In the standard approach, $I_\nu(\mu)$ is determined from a solution of equation (1) and $\bar{J}$ is calculated from equation (3) in angular and frequency integrations that involve a priori unknown dependences on these two variables. Determining the dependence of $I_\nu(\mu)$ on ν and μ is a major task for the solution of the radiative transfer equation. Deviations of the computed $I_\nu(\mu)$ from its exact angular shape and frequency profile contribute to the error in the computed $\bar{J}$ in each iteration. In contrast, the CEP method determines $\bar{J}$ from the integration in equation (7) that involves known dependences on both ν and μ; the dependence on these variables enters only from the optical depth $\tau_\nu(\mu)$, and it is a priori known from the input to the problem. The angular and frequency integrations are exact in the CEP method; the fact that the dependence of $I_\nu(\mu)$ on ν and μ is unknown is altogether irrelevant.

The other intrinsic strength of the CEP method is that it involves only level populations and thus takes full advantage of thermalization wherever that sets in. In contrast, the ALI technique must repeatedly solve the radiative transfer equation in the entire source, even in thermalized regions, to determine the radiation field everywhere.

5.1 Technicalities

The great efficiency of the Newton method in solving non-linear equations is another advantage of the CEP method. The prerequisite for a successful solution is a reasonable initial guess. An efficient strategy for working implementations of CEP is to start from the actual populations of a previous solution for similar physical conditions. A particularly useful approach is to start from the optically thin limit in which $p = 1$ everywhere and solve the level populations from the corresponding linear equations. The column density $\mathcal{N}$ is now increased in small steps until the desired value is reached, using in each step the populations from the previous one as the initial distribution. This technique can also work in the opposite direction – start from thermal equilibrium populations and a very large $\mathcal{N}$, and decrease $\mathcal{N}$ in small steps. An added advantage of this approach is that each step also provides information about the number of zones required for CEP convergence.

The Newton method requires inversion of the Jacobian matrix, and the number of operations in this process increases as the third power of the matrix dimension. Although this rapid rise did not have a serious effect in the examples presented here, it could degrade the performance in cases of very large numbers of levels and zones. Matrix inversion is avoided in the iterative scheme designed by van der Vorst (1992) for solution of the linear system of the Newton method. In this scheme, geared toward sparse Jacobian matrices, only the non-zero matrix elements are stored and used. We have experimented with this method and found it to be quite useful for the CEP technique. It is particularly suitable for multi-level problems because they tend to produce sparse matrices, as each level generally couples to only a limited number of other levels. Other alternatives are to use quasi-Newton schemes (e.g. Broyden's method) like those employed by Koesterke, Hamann & Kosmol (1992), or evolve the set of differential equations (34) until reaching steady state.

The efficiency of CEP computations can be further enhanced with better grid design. Our solutions of the semi-infinite atmosphere employed grids with equal logarithmic spacing in τ over 10 orders of magnitude, resulting in extremely thick zones deep inside the atmosphere. For example, even with $z = 600$, the zone thickness was $\tau = 1.7 \times 10^5$ in the $10^6 \leqslant \tau \leqslant 10^7$ region. These extremely thick zones do not pose any difficulties to CEP computations because they occur in regions where the populations are thermalized. Indeed, the zones could be even thicker in a much larger fraction of the source without compromising accuracy. It should thus be possible to achieve the same accuracy with fewer zones by concentrating them in the regions where the populations deviate from thermal equilibrium. Since the number of zones is the single most important factor in determining CEP runtime, a more sophisticated grid construction will make the method even more efficient. We intend to investigate the implementation of adaptive gridding algorithms in future work.

An additional increase in efficiency can be easily gained in practical applications that do not require the extreme precision we imposed in this comparative study. Here the functions α and β were calculated using the integral definition in equation (22), repeatedly performing highly accurate quadrature. Instead, one could employ the approximate series expansion derived by Capriotti (1965) for the function β. We have verified that this rapidly convergent series is always within 3 per cent of the exact result.[7] Another option is to calculate once a finely spaced table of the α- and β-functions and interpolate between its elements with an efficient algorithm.

5.2 CEP and ALI

The CEP method is suitable for solution also with the ALI approach. Starting from equation (3) in the operator form $\bar{J} = \Lambda S$, the ALI technique is based on the operator splitting $\Lambda = \Lambda^* + (\Lambda - \Lambda^*)$, where Λ^* is an approximation to the Λ operator. The mean intensity is obtained from the approximate expression $\bar{J} = \Lambda^* S + (\Lambda - \Lambda^*) S^{\rm prev}$ which involves the source function from the current and previous iterations. This approximation becomes exact upon convergence, when $S = S^{\rm prev}$. As already noted, it has been shown that the optimal choice for Λ^* is the diagonal of Λ.

Equation (6) gives $\bar{J} = (1 - p)S$, the Λ-operator form of the CEP method. From equation (17), the matrix elements of the CEP Λ-operator are simply

$$\Lambda_{ij} = (1 - \beta^i)\delta_{ij} - \frac{M^{ij}}{\tau^{i,i-1}}(1 - \delta_{ij}), \tag{38}$$

where δ_{ij} is the Kronecker delta. Thanks to the known dependence on ν and μ in the CEP approach, this expression allows the usage of approximate operators Λ^* of increasing complexity without any additional computational effort in the calculation of the matrix elements. In standard ALI techniques Λ^* is the diagonal of Λ, i.e. $\Lambda^*_{ij} = (1 - \beta^i)\delta_{ij}$. We have implemented this choice in an ALI solution of equation (23) and performed the two-level model calculations presented in this paper also with this technique. In all cases, the solution converged to exactly the same results as the algebraic CEP equations (27). Runtime for this ALI implementation of the CEP method was on a par with the SCP method up to 200 zones, but fell behind at larger z.[8] Given that in the CEP ALI implementation we have adopted the standard choice for Λ^*, the optimal choice in the CEP approach could well be different, improving the performance.

It is also important to point out that the CEP method could, in principle, be implemented in the framework of the Gauss–Seidel

[7] In Capriotti (1965), the small- and large-τ portions of the expansion were joined at line-centre optical depth $\tau_0 = 5$. They should be joined instead at $\tau_0 = 3.41$ for a smooth transition.

[8] We implemented the Ng (1974) acceleration technique to improve the convergence rate of the ALI method in both SCP and CEP.

and successive over-relaxation iterative methods. These methods were first applied in radiative transfer problems by Trujillo Bueno & Fabiani Bendicho (1995) using SCP as the formal solver. They can lead to an order of magnitude improvement in the number of iterations used to reach convergence, with a time per iteration that is virtually the same as the method based on the Jacobi iteration. Also of interest is the possibility of implementing the CEP method in the linear (Steiner 1991) or the non-linear (Fabiani Bendicho, Auer & Trujillo Bueno 1997) multi-grid methods. All of these issues will be addressed in future investigations.

5.3 Extensions

All the examples presented in this paper involved constant physical conditions. Variable conditions are handled by simply starting with zones that have constant physical conditions and proceeding to refine those divisions as required by the CEP solution accuracy. Equation (34) for the level populations already incorporates the handling of variable conditions by allowing the temperature and collision rates to vary between the zones.

For simplicity, our method was introduced in the context of a quiescent slab with the Doppler line profile. None of these simplifications represents an inherent limitation of the CEP method. The formal expressions do not specify the shape of $\Phi(x)$, and other line profiles can be implemented in just the same way. Extension from the slab to other geometries, although straightforward, requires some more work. Thanks to the planar symmetry, the angular variation of optical depth in a slab is simply $\tau(\mu) = \tau(\mu = 1)/\mu$, independently of either position or density profile. This symmetry does not carry to any other geometry; even in the case of spherical symmetry, the angular variation of τ cannot be calculated at any point other than the centre without specifying the density profile. However, generalizing the basic CEP relation equation (7) to handle any geometry is straightforward, and the fundamental advantage of integration over known frequency and angular variations remains intact. Finally, recalling that large velocity gradients was the context in which the escape probability approximation was originally introduced by Sobolev, the CEP method is well suited for exact handling of this case too.

The escape probability approach has been used in a number of simplified calculations of complex problems. These include: overlapping of spectral lines (so-called 'line fluorescence'), important for various ionic transitions (e.g. Bowen lines) in photoionized regions and OH lines in molecular clouds (Guilloteau, Lucas & Omont 1981; Elitzur & Netzer 1985; Lockett & Elitzur 1989); the effect of line overlap with underlying continuum (Netzer, Elitzur & Ferland 1985); and photoionization (Elitzur 1984). Importing these applications into the CEP framework is straightforward. Finally, another extension is the application of the CEP method to the self-consistent solution of the radiative transfer equations for polarized radiation and of the statistical equilibrium equations for the density matrix, the so-called non-local thermodynamic equilibrium problem of the second kind (see e.g. Landi Degl'Innocenti 2003; Trujillo Bueno 2003). We plan to provide these extensions in future publications.

5.4 Conclusions

While our new method outperforms the current leading techniques, its greatest advantage is its simplicity and ease of implementation. The CEP method employs a set of algebraic equations (equation 34) that are already incorporated in numerous widely used codes based on the escape probability approximation. All that is required for an exact solution with these existing codes is to augment the escape probability with the zone-coupling sum on the right-hand side of equation (35). With this simple modification, the multi-level line transfer problem is solved exactly.

ACKNOWLEDGMENTS

We thank Riccardo Cesaroni, Floris van der Tak and Stéphane Guilloteau for valuable remarks which helped us considerably in the preparation of this manuscript. This research was supported by NSF, NASA, the European Commission through the Solar Magnetism Network (contract HPRN-CT-2002-00313), and the Spanish Ministerio de Educación y Ciencia through project AYA2004-05792.

REFERENCES

Abramowitz M., Stegun I. A., 1972, Handbook of Mathematical Functions. Dover, New York
Apruzese J. P., Davis J., Dutson D., Whitney K. G., 1980, J. Quant. Spectrosc. Radiat. Transfer, 23, 479
Athay R. G., Skumanich A., 1971, ApJ, 170, 605
Auer L., Fabiani Bendicho P., Trujillo Bueno J., 1994, A&A, 292, 599
Avrett E. H., Hummer D. G., 1965, MNRAS, 130, 295
Avrett E. H., Loeser R., 1987, in Kalkofen W., ed., Numerical Radiative Transfer. Cambridge, Univ. Press, Cambridge, p. 135
Capriotti E. R., 1965, ApJ, 142, 1101
Carlsson M., 1991, in Crivellari L., Hubeny I., Hummer D. G., eds, Stellar Atmospheres: Beyond Classical Models. Kluwer, Dordrecht, p. 39
Caux E. et al., 1999, A&A, 347, L1
Dumont A.-M., Collin S., Paletou F., Coupé S., Godet O., Pelat D., 2003, A&A, 407, 13
Elitzur M., 1984, ApJ, 280, 653
Elitzur M., Netzer H., 1985, ApJ, 291, 464
Fabiani Bendicho P., 2003, in Hubeny I., Mihalas D., Werner K., eds, ASP Conf. Ser., Vol. 288, Stellar Atmosphere Modeling. Astron. Soc. Pac., San Francisco, p. 419
Fabiani Bendicho P., Auer L. H., Trujillo Bueno J., 1997, 324, 161
Guilloteau S., Lucas R., Omont A., 1981, A&A, 97, 347
Hubeny I., 1992, in Heber U., Jeffery C. S., eds, The Atmospheres of Early-Type Stars. Springer-Verlag, Berlin, p. 377
Jacobi C. G., 1845, Astron. Nachr., 32, 297
Koesterke L., Hamann W.-R., Kosmol P., 1992, A&A, 255, 490
Krolik J. H., McKee C. F., 1978, ApJS, 37, 459
Kunasz P. B., Auer L. H., 1988, J. Quant. Spectrosc. Radiat. Transfer, 39, 67
Landi Degl'Innocenti E., 2003, in Trujillo Bueno J., Moreno-Insertis F., Sánchez F., eds, Proc. XII Canary Islands Winter School of Astrophysics. Cambridge Univ. Press, Cambridge, p. 1
Lockett P., Elitzur M., 1989, ApJ, 344, 525
Netzer H., Elitzur M., Ferland G. J., 1985, ApJ, 299, 752
Ng K. C., 1974, J. Chem. Phys., 61, 2680
Olson G. L., Auer L. H., Buchler J. R., 1986, J. Quant. Spectrosc. Radiat. Transfer, 35, 431
Press W. H., Teukolsky S. A., Vetterling W. T., Flannery B. P., 1986, Numerical Recipes. Cambridge Univ. Press, Cambridge
Rybicki G. B., 1991, in Crivellari L., Hubeny I., Hummer D. G., eds, Stellar Atmospheres: Beyond Classical Models. Kluwer, Dordrecht, p. 1
Rybicki G. B., Hummer D. G., 1992, A&A, 262, 209
Steiner O., 1991, A&A, 242, 290
Tielens A. G. G. M., Hollenbach D., 1985, ApJ, 291, 722
Trujillo Bueno J., 2001, in Pilbratt G. L., Cernicharo J., Heras A. M., Prusti T., Harris R., eds, ESA SP-460, The Promise of the *Herschel Space Observatory*. ESA, Noordwijk, p. 261
Trujillo Bueno J., 2003, in Hubeny I., Mihalas D., Werner K., eds, ASP Conf. Ser. Vol. 288, Stellar Atmosphere Modeling. Astron. Soc. Pac., San Francisco, p. 551

Trujillo Bueno J., Fabiani Bendicho P., 1995, ApJ, 455, 646
van der Vorst H., 1992, SIAM J. Sci. Statist. Comput., 13, 631
van Noort M., Hubeny I., Lanz T., 2002, ApJ, 568, 1066
van Zadelhoff G.-J. et al., 2002, A&A, 395, 373

APPENDIX A: EXTERNAL RADIATION

The only effect of external radiation on the rate equations is to modify the exchange rate R^i_{ul} between levels u and l in the ith zone (see equation 12) according to

$$R^i_{ul} \Rightarrow R^i_{ul} - B_{ul}\bar{J}^i_{\rm e}\left(n^i_u - n^i_l\right), \tag{A1}$$

where $\bar{J}^i_{\rm e}$ is the zone average (as in equation 13) of the contribution of the external radiation to the local $\bar{J}$. When the external radiation corresponds to the emission from dust which permeates the source, $\bar{J}^i_{\rm e}$ is simply the angle-averaged intensity of the local dust emission in the ith zone. When the external radiation originates from outside the slab and has an isotropic distribution with intensity $I_{\rm e}(= J_{\rm e})$ in contact with the $\tau = 0$ face, then

$$\bar{J}^i_{\rm e} = \frac{1}{2} J_{\rm e} \frac{1}{\tau^{i,i-1}_{ul}} \left(\alpha^{i,0}_{ul} - \alpha^{i-1,0}_{ul}\right). \tag{A2}$$

When the slab is illuminated by parallel rays with intensity $I_{\rm e}(= 4\pi J_{\rm e})$ entering at direction (μ_0, ϕ_0) to the $\tau = 0$ face then

$$\bar{J}^i_{\rm e} = J_{\rm e} \frac{\mu_0}{\tau^{i,i-1}_{ul}} \left[\gamma\left(\tau^i_{ul}/\mu_0\right) - \gamma(\tau^{i-1}_{ul}/\mu_0)\right], \tag{A3}$$

where

$$\gamma(\tau) = \int_{-\infty}^{\infty} \left[1 - {\rm e}^{-\tau\Phi(x)}\right] {\rm d}x. \tag{A4}$$

This paper has been typeset from a TEX/LATEX file prepared by the author.